Small-strain shear modulus behavior from a laboratory scale cross-hole seismic test

C. Walton-Macaulay
Department of Civil & Environmental Engineering, Bucknell University, Lewisburg, PA, 17837, USA
J. Curd
GeoStabilization International, Williamstown, KY 41097, USA

ABSTRACT: Geotechnical engineering designs and analyses require assessments of the engineering properties of geomaterials used in geostructures. Increasingly, one of the engineering property being assessed of a geomaterial is the stiffness of soils. Key aspects of the soil stiffness is its influence on ground response and the deformation characteristics of many geostructures. Traditionally, estimates of stiffness were mostly done by triaxial tests with displacement transducers or by resonant column tests. Other methods are increasingly used today such as the bender element method, or field methods such as downhole tests, suspension logging, seismic reflection/refraction, spectral analysis of surface waves (SASW), and more commonly, cross-hole tests. These methods all measure the small-strain stiffness (or shear modulus) of the soil. A laboratory scale cross-hole method was performed and this paper presents the responsive small-strain stiffness behaviour of the unsaturated soil to soil compaction condition. Influences of dry density and void ratio on stiffness or shear wave velocity were paramount. Secondary influences of water content were noted though not well defined.

1 INTRODUCTION

The satisfactory performance of many engineering structures is dependent on the stiffness of the soil beneath. Researchers have considered the use of stiffness as a predictor of engineering properties (Hardin & Black 1968; Hardin & Drnevich 1972; Hardin & Kalinski 2005; Khosravi & McCartney 2009; Biglari et al. 2012). This stiffness property is derived from consideration of small strains, with relatively small amplitude and repeated loading and unloading due to vibrations (Hardin & Black 1968). Soil vibrations can be induced by loading from machine foundations, earthquakes, vehicular traffic and others. Figure 1 schematically illustrates some typical loading conditions and testing methods. Accurately predicting stiffness of soils during or soon after construction is essential to its performance and to developing a better understanding of soil modulus behavior.

Small-strain stiffness is analogous to small-strain shear modulus, in that as stiffness is related to the applied force and resulting soil deformation, and shear modulus is related to the applied shear stress and resulting shear strain, given a set of prescribed stress states. The cross-hole seismic method has been shown to be a suitable approach to determine soils small-strain behavior of shear wave velocities/modulus (Stokoe & Woods 1972). This method is scaled and used in the laboratory.

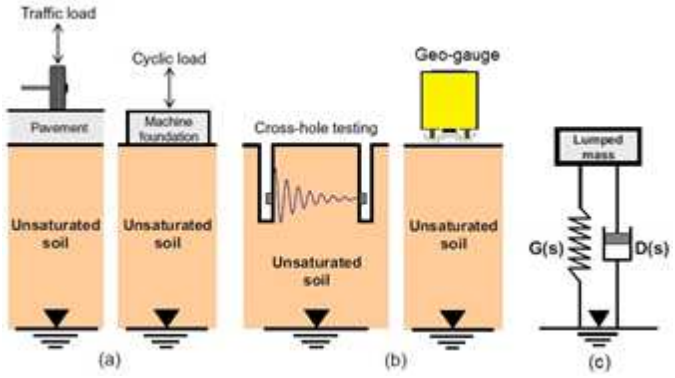

Figure 1. Unsaturated soil stiffness: (a) applications, (b) testing methods, (c) idealization (Hoyos et al. 2015).

This paper aims at studying the behavior of small-strain stiffness in a scaled laboratory test using the cross-hole seismic method. Since most conventional testing devices significantly underestimate small-strain behavior (Hoyos et al. 2015), this paper also aims to assess the suitability of the use of a portable geo-gauge to measure stiffness/modulus in the scaled laboratory tests. To accomplish these scaled tests, a laboratory test box was built and a series of cross-hole seismic and geo-gauge tests were performed under K_0 conditions on a clay soil compacted incrementally in the test box.

2 MATERIALS AND METHODS

2.1 *Soil type and index properties*

A naturally occurring soil formed from the parent rock and that is commonly used by the Kentucky Transportation Cabinet (KYTC), was selected for this study. Results from the sieve and hydrometer analysis, Atterberg limits and standard Proctor tests are tabulated in Table 1. The silty clay (CL-ML) soil was classified in accordance with the Unified Soil Classification System.

Table 1. Daviess County soil measured index properties.

Index property	
Grain size distribution	
Sand content (≤ 2 mm, %)	4.4
Percent silt & clay content (≤ 75 μm, %)	95.6
Clay content (≤ 2 μm, %)	21
Coefficient of uniformity	169.2
Coefficient of curvature	17.1
Specific gravity	2.72
Atterberg limits	
Plastic limit (%)	19
Liquid limit (%)	23
Plasticity index (%)	4
Unified soil classification system (USCS)	Silty clay CL-ML
Standard compaction tests	
Maximum dry density (kg/m^3)	1770.2
Optimum moisture content (%)	16.4

The soil water characteristic test conducted at standard Proctor compaction resulted in an air-entry value (AEV), residual suction (Ψ_r), and saturated gravimetric water content (w_{sat}) of 104 kPa, 3705 kPa, and 19.6% respectively. The curve and parameters are shown in Figure 2.

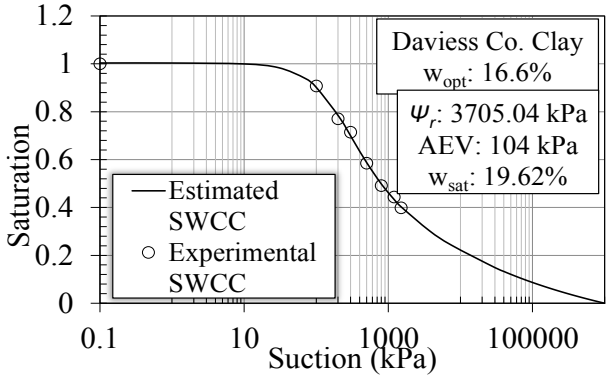

Figure 2. Estimated SWCC and experimental data.

The estimated SWCC was modeled using the Fredlund & Xing (1994) SWCC model with the resulting *a*, *n*, and *m* fitting parameters of 160.3672, 1.5425, and 0.6732 respectively. The Fredlund and Xing (1994) SWCC model is given as follows:

$$w_w = \frac{\ln\left[1+\left(\frac{\psi}{\psi_r}\right)\right]}{\ln\left[1+\left(\frac{1{,}000{,}000}{\psi_r}\right)\right]} \frac{w_s}{\left\{\ln\left[e+\left(\frac{\psi}{a}\right)^n\right]\right\}^m} \quad (1)$$

2.2 *Test equipment*

The test box used is described in detail in Walton-Macaulay et al. (2017). A brief description is provided here for reading convenience. The test box was constructed of wood with interior dimensions of length 38.6 cm, width 38.4 cm and height 34.8 cm. It was braced by steel plates and bars to limit the lateral deflection, for an assumption of K_0 condition.

Earth pressure cells, with accuracy of 0.1 percent of full scale, were placed such that load transfer measurements can be made in three major axes. Two pressure cells with 350 kPa maximum capacity were placed vertically and flat against two adjacent sides for lateral pressure measurement and the third (1 MPa maximum capacity) placed horizontally and flat on the bottom of the test box for vertical transfer pressure measurements. A hydraulic load frame with maximum capacity of 1334 kN was used to compact the bulk soil sample placed in the test box. An oscilloscope capable of measuring analog and digital signals of up to 200 and 100 MHz respectively was used to determine the shear wave velocities in a cross-hole seismic formation. The cross-hole seismic formation included two copper hollow rods placed at opposite corners of the test box for the source and receiver positions. A metal rod with a tip wedge was used with a hammer to generate the source waves. The hammer was connected to the oscilloscope. An accelerometer connected to the oscilloscope was used in the receiver position.

A Geo-gauge capable of measuring stiffness electro-mechanically was used. This Geo-gauge, manufactured by Humbolt, Inc., imparts very small displacement of less than 1.27×10^{-3} mm to the soil surface where placed, and it does so at different frequencies from 100 kHz to 196 kHz.

2.3 *Preparation and procedure*

The bulk soil was prepared at a constant moisture content by initially air drying or obtaining a hygroscopic moisture, then water added and the bulk soil mixed to achieve a target constant moisture content. The bulk specimen was sealed and stored for a minimum of 24 hours to allow for moisture equilibrium prior to testing. Four different constant moistures were targeted for each test sequence with two bulk specimens prepared at below optimum moisture content for standard compaction, one at optimum moisture content, and the fourth at above the optimum moisture content.

For each prepared bulk specimen at constant moisture content, the bulk soil was placed in the test box and statically compacted to incremented and reduced heights targeted to 38, 64, 90, 115 and 140 mm below the initial height. The static load was applied at a strain rate of 5.08 mm/min. Walton-Macaulay et al. (2017) indicated that a non-uniform behaviour is attributed to dynamically compacted soils due to destruction of inter-particle forces, and since uniformity was of great importance for this study, a static compaction method was selected for this study. After each incremental compaction, the soil was unloaded and allowed to rebound to an equilibrium point established as a change in residual pressures (read from the earth pressure cells) of less than 0.041 kPa/min.

Shear wave velocities were obtained from the cross-hole seismic tests following the rebound of the soil after every incremental compaction. The schematic diagram in Figure 3 shows the idealized setup of the cross-hole seismic test. The metal rod with the wedge-tip and the accelerator were placed in their respective positions and to the desired test depth which was generally at the centre of the compacted soil height. The hammer was used to uni-axially strike the top of the wedge-tip rod and excite wave propagation within the bulk soil. The accelerometer placed vertically, thereby predominantly receiving shear waves. The oscilloscope logs both the transmitted wave and the received shear wave.

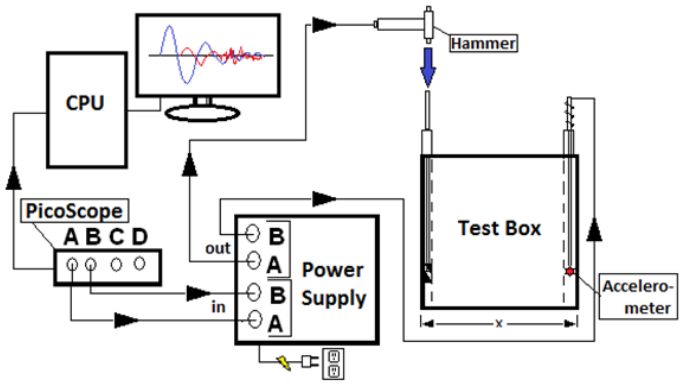

Figure 3. Schematics of the cross-hole seismic equipment set-up.

The shear wave velocity, V_s was determined as shown in Equation 2, and the shear modulus, G was determined as shown in Equation 3.

$$V_s = \frac{Wave\ travel\ length}{Travel\ time} = \frac{L}{t} \tag{2}$$

$$G = (Total\ density)(Shear\ wave\ velocity)^2 = \rho V_s^2 \tag{3}$$

Small-strain stiffness measurements were made using the Geo-gauge following the incremental compaction/rebound of the soil. Two measurements were made and averaged with the second made at a rotated 90 degrees from the first location. The averaged small-strain stiffness, k value was then used to obtain the elastic (Young's) modulus based on the Geo-gauge ring foot's radius, R and the soil's Poisson's ratio, v using Equation 4. Thereafter the shear modulus was determined using elastic theory relationship as shown in Equation 5.

$$E = k\frac{(1-v^2)}{1.77R} \tag{4}$$

$$G = E\frac{(1-v)}{2(1+v^2)} \tag{5}$$

3 RESULTS AND ANALYSES

The vertical and lateral transfer stresses measured by the earth pressure cells are considered to be the principal stresses due to the reduced friction of the cells' polished finish surface, the horizontal soil surface, and the parallel and perpendicular orientation of the cells to the uni-axial loading. The measured stresses are the vertical stress, σ_1 and the lateral stresses, σ_2 and σ_3. The net mean stress with respect to pore-air pressure is the mean stress assuming that the pore-air pressure during testing is zero. The net mean stress, p is therefore given as follow:

$$p = p_{net} = p_{mean} = \frac{\sigma_1 + \sigma_2 + \sigma_3}{3} \tag{6}$$

The internal stress resident in the soil structure after all applied forces has been removed and the soil allowed to rebound is the residual net mean stress. Residual stress is present in compacted soil, but are more pronounced in soils compacted under K_0 conditions, and therefore can have significant effects on soil behavior.

3.1 *Dynamic response*

Cross-hole seismic tests were performed under loading and residual stress conditions. The time of first arrival was used in determining the travel time from the initial excited wave propagated to when it was initially received by the accelerometer.

Figure 4 shows the behavior of the shear modulus data determined from the cross-hole seismic test under loading conditions. This shear modulus from the cross-hole seismic test is represented as G_{CH}. It is clear that the shear modulus generally increases with net mean stress, which is consistent with other studies using different methods such as bender elements and resonant columns (Nyunt et al. 2011; Hoyos et al. 2015).

At the moisture content of 16.6 percent, there is a significant increase of G_{CH} very early on or under low net mean stress. This moisture content is very

close to the target optimum moisture content of 16.4 percent under standard compaction conditions. With conditions of optimum moisture content, the soil lends itself to become a more readily compacted soil structure. Significant shear modulus increases in the soils dry of optimum moisture content (11.4 and 13.2 percent) but only after the loading is above 100 kPa. As expected for the soil above optimum moisture content, the shear modulus is relatively lower than the other soils, but with notable increases with net mean stress under load.

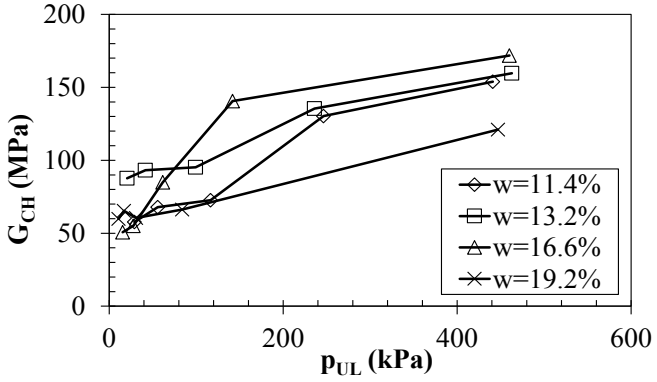

Figure 4. Shear modulus with net mean stress under load.

To assess the behavior of the compacted soil ascompacted the residual stress has to be considered without the applied load used to compact it. Figure 5 shows the behavior of the shear modulus data determined from the cross-hole seismic test under residual stress conditions. The data is not as well defined as that under load, but shear modulus generally increases with residual net mean stress, which is consistent with Heitor et al. (2013). Of note are the significant differences in the behavior of the soil that is wet of optimum moisture content relative to the soils that are at and lower of optimum moisture content.

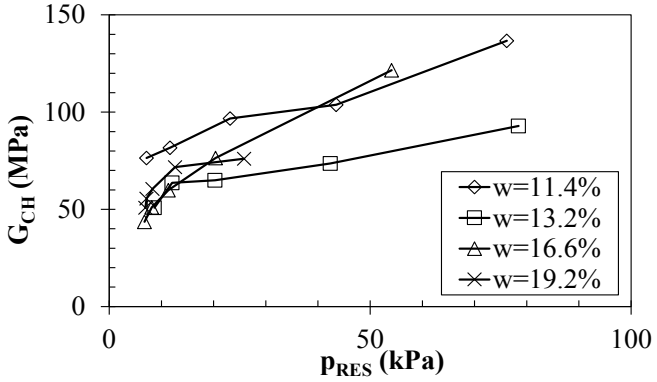

Figure 5. Shear modulus with residual net mean stress.

In Figure 5, the maximum residual net mean stress for the soil above optimum moisture content (19.2 percent), is significantly smaller than the maximum residual net mean stress of the other soils and the shear modulus appear to be close to a threshold maximum. In other words, the internal (residual) stresses are not 'locked' in and dissipates to a much lower internal stress. This is most likely due to the wetter soil's dispersed structure and higher degree of saturation.

From Figure 5, the maximum residual net mean stress for the soils dry of optimum moisture were just under 80 kPa, about 55 kPa at optimum moisture and about 25 kPa wet of optimum moisture content. The relatively higher residual net mean stress were the results of high residual lateral stresses that remain even after the external compaction loads are removed. These internal residual lateral stresses can significantly affect soil behavior and therefore the structural support they may provide. These residual stresses were assessed and evaluated by considering the coefficient of the earth pressure at rest, K_0, which is defined as the ratio of the in-situ horizontal effective stresses σ_2, and σ_3, to the in-situ vertical effective stress σ_2, when the vertical and horizontal directions are coincident with those of the principal stresses (Terzaghi 1920; 1925).

Figure 6 shows the averaged K_0 with net mean stress for the loading and residual conditions. It is clear that K_0 under loading conditions increases slightly while in a relatively loose condition (low net mean stress range of 10-30 kPa) and can be assumed to remain relatively constant with increasing net mean stress, with exception that the wetter soil may see slight increases in K_0 at higher net mean stress. Since K_0 is relatively constant, it can be assumed that the loading transfer mechanisms with the soil structure is not dependent on the direction of transfer. Therefore, for external load increases, the magnitude of distributed loads is equivalent in the horizontal and vertical directions.

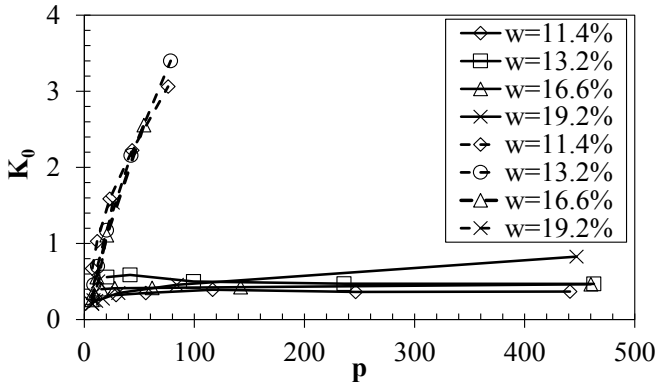

Figure 6. Coefficient of earth pressure at rest with net mean stress.

It is also clear that K_0 under residual conditions increases rapidly with values approaching passive earth pressure conditions for the soils dry of optimum moisture content and the soil close to optimum moisture content. This indicates that higher magnitudes of lateral stresses are retained in the soil structure especially for a flocculated (drier) soil structure

than for a dispersed (wetter) state. The rate of increase of K_0 for residual conditions appear unaffected by moisture content.

The horizontal and vertical stresses for the two conditions of under load and after load (residual) were compared and the comparative data presented in Figure 7. The linear trends indicate a consistent ratio in the increase of stresses under load to the consequential residual stresses. Figure 7a shows the vertical stress and the horizontal stresses for the test soil with 11.4 percent moisture content. This data trend is typical and therefore only this data shown here for brevity. Figure 7a indicates that the vertical stress is more dominant under loading (lower slope) and the residual stresses become more significant in the horizontal or lateral direction (higher slopes). The ratio of the stresses under load to the residual stresses is of a magnitude difference for σ_1 (about 1/30) and for σ_2 and σ_3, (about 1/3).

Figure 7b shows the comparison for only the vertical stresses, which shows a fairly consistent trend across moisture contents. As an exception, the wetter soil appears to show that at a point, increases in the external vertical stress does not cause further increase in residual vertical stress.

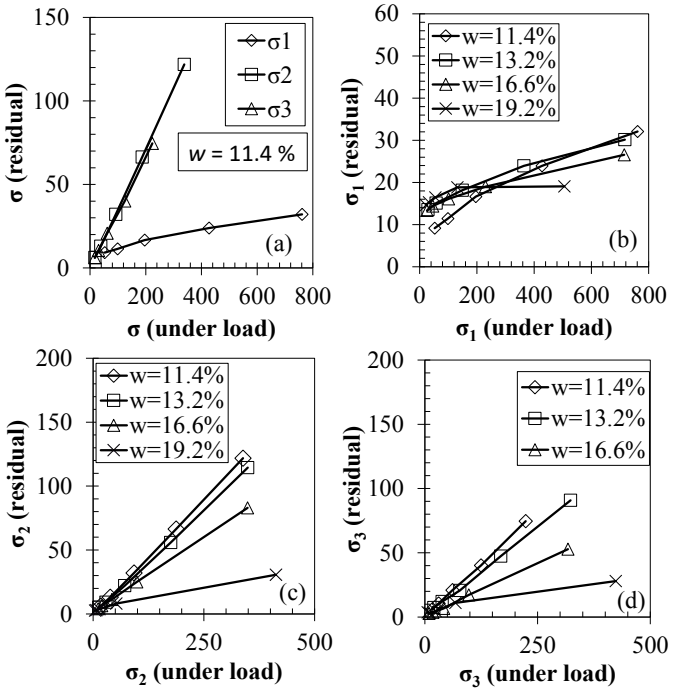

Figure 7. Comparative vertical and horizontal stress analysis.

Figure 7c and 7d show the comparisons for the lateral stresses, which indicates a dependency on moisture content. Assuming linearity, the ratio of the lateral stresses under load to the lateral residual stresses can be approximated as 6/16, 5/16, 3/16 and 1/16 at moisture contents of 11.4, 13.2, 16.6, and 19.2 percent respectively. The decreasing ratios indicates that drier soils retain, more of their internal lateral stress caused by compaction loading as residual stresses.

Contrary to these higher positive stresses, drier soils also experiences higher negative pore-water stresses u_w, due to their capillary and adsorptive properties, however these negative pore-water stresses can be represented as matric suction stresses, (u_a - u_w) in reference to the pore-air pressure stress u_a. Therefore, in unsaturated soils (matric suction present), the magnitude of lateral (horizontal) stress is reduced. Estimates of K_0 can be made considering elastic equilibrium within a homogeneous, isotropic soil mass. One suggested model includes the matric suction parameter developed by Fredlund et al. (2012) which is given in terms of the elastic modulus with respect to a net external stress, E, and the elastic modulus with respect to the matric suction, H. Substituting E for G in Equation 5, the K_0 is as follows:

$$K_0 = \frac{v}{1+v} - \left[\frac{2G}{H}\frac{\left(1+v^2\right)}{\left(1-v\right)^2}\frac{\left(u_a-u_w\right)}{\left(\sigma_v-u_a\right)}\right] \quad (7)$$

where v is the Poisson's ratio. (u_a - u_w) and H were determined from estimated data presented by Walton-Macaulay et al. (2017) for this soil at different void ratios, under the same test conditions.

Figure 8 shows the comparison of the estimated and experimental data of K_0 under load. One of the data points is considered to be an outlier due to the low estimated value (close to zero), indicating an impending cracking of the soil. Though there are some deviations from the line of unity, the model provides reasonable estimates of experimental values. Poor estimates of K_0 under residual conditions were made and not reported in this study.

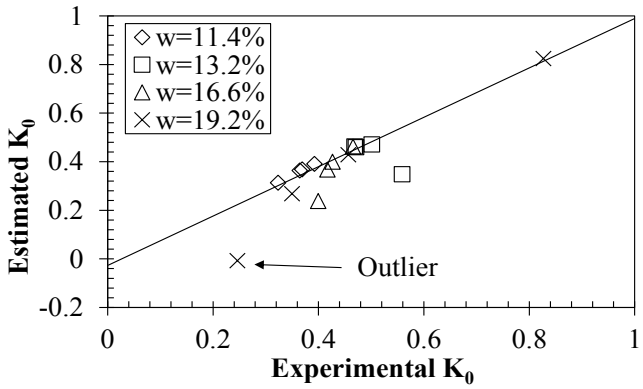

Figure 8. Comparative K_0 from experimental and estimated data.

The shear modulus determined from the use of the Geogauge were compared with the shear modulus from the cross-hole seismic tests. Figure 9 shows the comparison of all experimental values of G at different moisture contents. The Geogauge presents shear modulus that are consistently lower than the cross-hole seismic shear modulus, which may be partially due to the location of the tests (surface vs. at depth), and to the confinement of the test box.

Additional work is necessary to confirm the suitability of the use of a Geogauge in a laboratory setting.

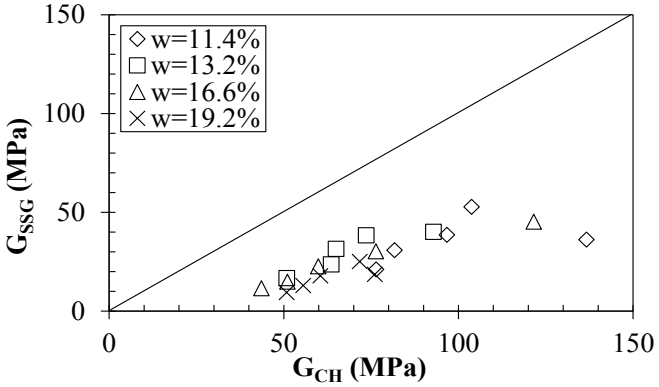

Figure 9. Comparison of G response from cross-hole seismic and Geogauge tests.

4 CONCLUSIONS

An attempt to study the behavior of small-strain shear modulus of a silty clay soil was made on the basis of performing a scaled cross-hole seismic testing in the laboratory. A test box was used that allowed for uni-axial static loading to achieve incremental compaction of the bulk soils at different constant moisture contents. The results show that shear modulus increases in both conditions of under loading to achieve the compaction and under residual conditions after the loading had been removed and the soil allowed to rebound.

The coefficient of earth pressure at rest K_0, was assessed and under loading conditions, though it increases slightly in the low net mean stress range, K_0 remained relatively constant with increasing net mean stress. The exception to having the relatively constant K_0 is that though minimal, the wetter soil showed continued increase in K_0 at higher net mean stress. As such, in a predominant particle contact aggregation structure (drier soils), the distribution of load/stress transfer is not dependent on its direction.

Under residual conditions, K_0 increases rapidly with increasing residual net mean stress and approaching passive earth pressure conditions. Under residual conditions, predominant particle contact aggregation soil structure retain higher magnitudes of lateral stresses from the external stress used to obtain compaction. The rate of increase of K_0 for residual conditions appear unaffected by moisture content.

The residual stresses, also increased with increased residual net mean stress, a result of increased compaction energy. Lateral residual stresses decreased with increasing moisture content. A comparison shows that lateral stresses are more dependent of the moisture content, than vertical stresses.

Reasonable estimates of K_0 under loading can be made using the Fredlund et al. 2012 unsaturated model, even though estimates of matric suction were used. This model poorly estimated K_0 for residual conditions therefore were not reported. Further research into residual K_0 is necessary.

Finally, the shear modulus obtained from the use of a Geogauge are consistently lower than shear modulus obtained from the cross-hole seismic tests. This is partially attributed due to the location of the tests which was performed at the soils surface for the Geogauge and at mid-depth of the soil for the cross-hole seismic tests.

5 ACKNOWLEDGEMENTS

The lead author appreciates the support of Bucknell University, especially the time allowed away from teaching to focus on research and writing this paper.

6 REFERENCES

Biglari, M., d'Onofrio, A., Mancuso, C., Jafari, M.K., Shafiee, A., & Ashayeri, I. 2012. Small-strain Stiffness of Zenoz kaolin in unsaturated conditions. *Canadian Geotechnical Journal* 49(3): 311-322.

Hardin, B.O., & Black, W.L. 1968. Vibration modulus of normally consolidated clay. *Journal of the Soil Mechanics and Foundation Division* 94(2): 353-369.

Hardin, B.O., & Drnevich, V.P. 1972. Shear modulus and damping in soils: measurement and parameter effects. *Journal of the Soil Mechanics and Foundation Division* 98(6): 603-624.

Hardin, B.O., & Kalinski, M.E. 2005. Estimating the Shear Modulus of Gravelly Soils. *Journal of Geotechnical and Geoenvironmental Engineering* 131(7): 867-875.

Khosravi, A., & McCartney, J.S. 2009. Impact of stress state on the dynamic shear moduli of unsaturated, compacted soils. *4th Asia-Pacific Conference on Unsaturated Soils*. Newcastle, Australia. Nov. 23-25, 2009.

Fredlund, D.G., Rahardjo, H., & Fredlund, M.D. 2012. Unsaturated soil mechanics in engineering practice. *John Wiley & Sons, Inc.*, Hoboken, New Jersey.

Heitor, A., Indraratna, B., & Rujikiatkamjorn, C. 2013. Laboratory study of small-strain behavior of a compacted silty sand. *Canadian Geotechnical Journal* 50(2): 179-188.

Hoyos, L.R., Suescun-Florez, E.A., & Puppala, A. 2015. Stiffness of intermediate unsaturated soil from simultaneous suction-controlled resonant column and bender element testing. *Engineering Geology* 188: 10-28.

Nyunt, T.T., Leong, E.C., & Rahardjo, H. 2011. Strength and small-strain stiffness characteristics of unsaturated sand. *Geotechnical Testing Journal* 34(5): 551-561.

Stokoe, K.H., II & Woods, R.D. 1972, In Situ Shear Wave Velocity by Cross-Hole Method. *Journal of the Soil Mechanics and Foundations Division, ASCE* 98(5): 443-460.

Walton-Macaulay, C., Bryson, L.S., & Curd, J. 2017. Compacted unsaturated soil behaviour in a large scale laboratory test. *2nd Pan-American Conference on Unsaturated Soils*, Dallas, TX, Nov. 12-15, 2017.

Terzaghi, K. 1920. Old earth pressure theories and new test results. *Engineering News Record* 85: 632-637.

Terzaghi. K. 1925. Principles of soil mechanics. *Engineering News Record* 95: 796-800.